Inclusive Lambda Production
in Two-Photon Collisions at LEP

The L3 Collaboration

Abstract

The reactions $e^+e^- \rightarrow e^+e^-\Lambda X$ and $e^+e^- \rightarrow e^+e^-\overline{\Lambda}X$ are studied using data collected at LEP with the L3 detector at centre-of-mass energies between 189 and 209 GeV. Inclusive differential cross sections are measured as a function of the lambda transverse momentum, p_t, and pseudo-rapidity, η, in the ranges 0.4 GeV $< p_t < 2.5$ GeV and $|\eta| < 1.2$. The data are compared to Monte Carlo predictions. The differential cross section as a function of p_t is well described by an exponential of the form $A\exp(-p_t/\langle p_t \rangle)$.

Submitted to *Phys. Lett. B*

1 Introduction

Two-photon collisions are the main source of hadron production in high-energy e^+e^- interactions at LEP via the process $e^+e^- \rightarrow e^+e^-\gamma^*\gamma^* \rightarrow e^+e^-hadrons$. The outgoing electron and positron carry almost the full beam energy and their transverse momenta are usually so small that they escape, undetected, along the beam pipe. In this process, the negative four-momentum squared of the photons, Q^2, has an average value $\langle Q^2 \rangle \simeq 0.2$ GeV^2 and they can therefore be considered as quasi-real. In the Vector Dominance Model (VDM), each photon can transform into a vector meson with the same quantum numbers, thus initiating a strong interaction process with characteristics similar to hadron-hadron interactions. This process dominates in the "soft" interaction region, where hadrons are produced with a low transverse momentum, p_t. Hadrons with high p_t may also be produced by the QED process $\gamma\gamma \rightarrow q\overline{q}$ (direct process) or by QCD processes originating from the partonic content of the photon (resolved processes).

The L3 Collaboration has previously studied inclusive π^0, K_S^0 [1] and charged hadron [2] production in quasi-real two-photon collisions. In this Letter, the inclusive Λ and $\overline{\Lambda}$ production[1] from quasi-real photons is studied for a centre-of-mass energy of the two interacting photons, $W_{\gamma\gamma}$, greater than 5 GeV. The results are expressed in bins of transverse momentum, p_t, and pseudo-rapidity, η, in the ranges 0.4 GeV $< p_t <$ 2.5 GeV and $|\eta| < 1.2$. The η range is further divided in two subsamples with 0.4 GeV $< p_t \leq 1$ GeV and 1 GeV $< p_t <$ 2.5 GeV. The data sample corresponds to a total integrated luminosity of 610 pb^{-1} collected with the L3 detector [3], at e^+e^- centre-of-mass energies $\sqrt{s} = 189 - 209$ GeV, with a luminosity weighted average value of $\sqrt{s} = 198$ GeV . Results on inclusive Λ production for a smaller data sample at lower $\sqrt{s}$ were previously reported by the TOPAZ Collaboration in the range 0.75 GeV $< p_t <$ 2.75 GeV [4]. The H1 Collaboration investigated the Λ photoproduction at HERA [5].

2 Monte Carlo simulation

The process $e^+e^- \rightarrow e^+e^-hadrons$ is modelled with the PYTHIA [6] and PHOJET [7] event generators with two times more luminosity than the data. Both generators include the VDM, direct and resolved processes. In PYTHIA, including these processes for each photon leads to six classes of interactions. A smooth transition between these classes is then obtained by introducing a transverse momentum scale. The two-photon luminosity function is based on the EPA approximation [8] with a cut at the mass of the rho meson. The SaS-1D parametrisation is used for the photon structure [9]. PHOJET relies on the Dual Parton Model [10], with a soft and a hard component. The two-photon luminosity functions is calculated in the formalism of Reference 8. The leading-order GRV parametrisation is used for the photon structure [11]. For both programs, matrix elements are calculated at the leading order and higher-order terms are simulated by parton shower in the leading-log approximation. The fragmentation is performed using the Lund string fragmentation scheme as implemented in JETSET [6], which is also used to simulate the hadronisation process. The strangeness suppression factor in JETSET is chosen as 0.3, while a value $\alpha_S(m_Z) = 0.12$ is used for the strong coupling constant.

From a study of Monte Carlo events, the hard component is found to be larger than the soft component. Their ratio goes from around two at low values of p_t to around three at high values of p_t.

---

[1] If not mentioned otherwise, the symbol Λ refers to both Λ and $\overline{\Lambda}$, as both charge conjugate final state are analysed.

The following Monte Carlo generators are used to simulate the background processes: KK2f [12] for the annihilation process $e^+e^- \to q\overline{q}(\gamma)$; KORALZ [13] for $e^+e^- \to \tau^+\tau^-(\gamma)$; KORALW [14] for $e^+e^- \to W^+W^-$ and DIAG36 [15] for $e^+e^- \to e^+e^-\tau^+\tau^-$. The response of the L3 detector is simulated using the GEANT [16] and GHEISHA [17] programs. Time dependent detector inefficiencies, as monitored during each data taking period, are included in the simulations. All simulated events are passed through the same reconstruction program as the data.

3   Event selection

Two-photon interaction events are mainly collected by the track triggers [18], with a low transverse momentum threshold of about 150 MeV, and the calorimetric energy trigger [19]. The selection of $e^+e^- \to e^+e^- hadrons$ events [20] is based on information from the central tracking detectors and the electromagnetic and hadronic calorimeters. It consists of:

- A multiplicity cut. To select hadronic final states, at least six objects must be detected, where an object can be a track satisfying minimal quality requirements or an isolated calorimetric cluster of energy greater than 100 MeV.

- Energy cuts. The total energy deposited in the calorimeters must be less than 40% of $\sqrt{s}$ to suppress events from the $e^+e^- \to q\overline{q}(\gamma)$ and $e^+e^- \to \tau^+\tau^-(\gamma)$ processes. In addition, the total energy in the electromagnetic calorimeter is required to be greater than 500 MeV in order to suppress beam-gas and beam-wall interactions and less than 50 GeV to remove events from the annihilation process $e^+e^- \to q\overline{q}(\gamma)$.

- An anti-tag condition. Events with a cluster in the luminosity monitor, which covers the angular region 31 mrad $< \theta <$ 62 mrad, with an electromagnetic shower shape and energy greater than 30 GeV are excluded from the analysis. In addition, events with an electron scattered above 62 mrad are rejected by the energy cuts.

- A mass cut. The invariant mass of all visible particles, W_{vis}, must be greater than 5 GeV. In this calculation, the pion mass is attributed to tracks while isolated electromagnetic clusters are treated as massless. The distribution of W_{vis} for data and Monte Carlo after all other cuts are applied is shown in Figure 1. Values of W_{vis} up to 200 GeV are accessible.

About 3 million hadronic events are selected by these criteria with an overall efficiency of 45%. The background level of this sample is less than 1% and is mainly due to the $e^+e^- \to q\overline{q}(\gamma)$ and $e^+e^- \to e^+e^-\tau^+\tau^-$ processes. The background from beam-gas and beam-wall interactions is found to be negligible.

The Λ baryons are reconstructed using the decay $\Lambda \to p\pi$. Secondary decay vertices are selected which are formed by two oppositely charged tracks. The secondary vertices must satisfy the following criteria:

- The distance, in the plane transverse to the beam direction, between the secondary vertex and the primary e^+e^- interaction point must be greater than 3 mm.

- The angle between the total transverse momentum vector of the two outgoing tracks and the direction in the transverse plane between the primary interaction point and the secondary vertex must be less than 100 mrad.

3

The distributions of these variables are presented in Figure 2. The proton is identified as the track with the largest momentum. Monte Carlo studies show that this association is correct for more than 99% of the vertices. In addition, the dE/dx measurement of both proton and pion candidates must be consistent with this hypothesis with a confidence level greater than 0.01.

After these cuts, about 70000 events are selected. The distribution of the invariant mass of the pπ system, $m(p\pi)$, shows a clear Λ peak, as shown in Figures 3 and 4 for the different p_t bins listed in Table 1. The resolution of $m(p\pi)$ is found to be around 3 MeV and is well reproduced by Monte Carlo simulations.

4   Differential cross sections

The differential cross sections for Λ production as a function of p_t and $|\eta|$ are measured for $W_{\gamma\gamma} > 5$ GeV, with a mean value of 30 GeV, and a photon virtuality $Q^2 < 8$ GeV^2 with $\langle Q^2 \rangle \simeq 0.2$ GeV^2. This phase space is defined by cuts at the generator level of the Monte Carlo.

The number of Λ baryons in each p_t and $|\eta|$ bin is evaluated by means of a fit to the $m(p\pi)$ spectrum in the interval 1.085 GeV $< m(p\pi) < 1.145$ GeV. The signal is modelled with a Gaussian and the background by a fourth-degree Chebyshev polynomial. All parameters, including the mass and width of the peak, are left free. The results are given in Tables 1, 2 and 3.

The overall efficiencies, also listed in Tables 1, 2 and 3, include reconstruction and trigger efficiencies and take into account the 64% branching fraction of the decay $\Lambda \to p\pi$. The reconstruction efficiency, which includes effects of the acceptance and the selection cuts, is calculated with the PHOJET and PYTHIA Monte Carlo generators. As both generators reproduce well the shapes of the experimental distributions of hadronic two-photon production [20], their average is used to calculate the selection efficiency. The efficiency does not depend on the Q^2 cut-off. The track trigger efficiency is calculated for each data taking period by comparing the number of events accepted by the track and the calorimetric energy triggers. The efficiency of the higher level triggers is measured using prescaled events. The total trigger efficiency increases from 82% for $p_t < 0.4$ GeV to 85% in the high p_t region.

The differential cross section as a function of p_t is first measured for the three different data samples collected in 1998, 1999 and 2000 at different values of $\sqrt{s}$ and for different trigger and machine background conditions. Good agreement is obtained between the three measurements. The different data samples are therefore combined into a single data sample.

Sources of systematic uncertainties on the cross section measurements are: background subtraction, scale and resolution uncertainties, Monte Carlo modelling and the accuracy of the trigger efficiency measurement. Their contributions are listed in Table 4. The dominant source of systematic uncertainty is due to background subtraction. It is estimated using different background parameterizations and fit intervals in the fitting procedure. The scale and resolution uncertainties are assessed by varying the selection cuts. The main contributions arises from the secondary vertex selection (3.2%) and the proton and pion identification criteria (2.5%). The uncertainty due to the selection of e$^+$e$^- \to$ e$^+$e$^-$*hadrons* events is 1%. The Monte Carlo modelling uncertainty, taken as half the relative difference between PHOJET and PYTHIA, increases with p_t from 1% to 5%. A systematic uncertainty of 2% is assigned to the determination of the trigger efficiency, which takes into account the determination procedure and time stability.

5 Results

The average multiplicity of Λ baryons in the range $W_{\gamma\gamma} > 5$ GeV, 0.4 GeV $< p_t < 2.5$ GeV and $|\eta| < 1.2$ is $(1.57 \pm 0.11) \times 10^{-2}$ per $e^+e^- \rightarrow e^+e^- hadrons$ event. The uncertainty includes both statistical and systematic uncertainties. This result is below the value $(1.80 \pm 0.01) \times 10^{-2}$ predicted by PHOJET and above the value $(1.43 \pm 0.01) \times 10^{-2}$ predicted by PYTHIA. The ratio of Λ to $\overline{\Lambda}$ baryons, as determined from the charge of the most energetic track of the vertex, is found to be $N(\overline{\Lambda})/N(\Lambda) = 0.99 \pm 0.04$.

The sum of the differential cross sections for the $e^+e^- \rightarrow e^+e^-\Lambda X$ and $e^+e^- \rightarrow e^+e^-\overline{\Lambda}X$ processes as a function of p_t for $|\eta| < 1.2$ is presented in Table 1 and Figure 5. Mass effects explain the lower value obtained in the first bin. The behaviour of the cross section for 0.75 GeV $< p_t < 2.5$ GeV is well described by an exponential of the form $A \exp(-p_t/\langle p_t \rangle)$, as shown in Figure 5a, with a mean value $\langle p_t \rangle = 368 \pm 17$ MeV. For comparison, the values $\langle p_t \rangle \simeq 230$ MeV and $\langle p_t \rangle \simeq 290$ MeV are obtained for inclusive π^0 and K_S^0 production, respectively [1].

The data are compared to the PHOJET and PYTHIA Monte Carlo predictions in Figure 5b. The region $p_t < 0.6$ GeV is well described by PYTHIA, whereas PHOJET overestimates the cross section. On the contrary, the region 0.6 GeV $\leq p_t \leq 1$ GeV is better reproduced by PHOJET while PYTHIA lies below the data. For $p_t > 1$ GeV both PYTHIA and PHOJET underestimate the data. This level of agreement is not unusual in two-photon physics.

The differential cross sections as a function of $|\eta|$ for 0.4 GeV $< p_t \leq 1$ GeV and 1 GeV $< p_t < 2.5$ GeV are given in Tables 2 and 3 and shown in Figure 6. Both Monte Carlo programs describe well the almost uniform η shape, while the size of the discrepancy on the absolute normalization depends on the p_t range.

References

[1] L3 Collab., P. Achard *et al.*, Phys. Lett. **B 524** (2002) 44.

[2] L3 Collab., P. Achard *et al.*, Phys. Lett. **B 554** (2003) 105.

[3] L3 Collab., B. Adeva *et al.*, Nucl. Instr. Meth. **A 289** (1990) 35;
L3 Collab., O. Adriani *et al.*, Phys. Rept. **236** (1993) 1;
M. Chemarin *et al.*, Nucl. Instr. Meth. **A 349** (1994) 345;
M. Acciarri *et al.*, Nucl. Instr. Meth. **A 351** (1994) 300;
I. C. Brock *et al.*, Nucl. Instr. Meth. **A 381** (1996) 236;
A. Adam *et al.*, Nucl. Instr. Meth. **A 383** (1996) 342.

[4] TOPAZ Collab., R. Enomoto *et al.*, Phys. Lett. **B 347** (1995) 179.

[5] H1 Collab., C. Adloff *et al.*, Z. Phys. **C 76** (1997) 213.

[6] PYTHIA version 5.722 and JETSET version 7.409 are used with default options;
T. Sjöstrand, Comp. Phys. Comm. **82** (1994) 74.

[7] PHOJET version 1.05c is used with default options;
R. Engel, Z. Phys. **C 66** (1995) 203;
R. Engel and J. Ranft, Phys. Rev. **D 54** (1996) 4244.

[8] V.M. Budnev *et al.*, Phys. Rept. **15** (1974) 181.

[9] G. Schuler and T. Sjöstrand, Z. Phys. **C 68** (1995) 607.

[10] A. Capella *et al.*, Phys. Rep. **236** (1994) 225.

[11] M. Gluck, E. Reya and A. Vogt, Phys. Rev. **D 45** (1992) 3986;
Phys. Rev.**D 46** (1992) 1973.

[12] KK2f version 4.12 is used;
S. Jadach, B. F. L. Ward and Z. Wąs, Comp. Phys. Comm. **130** (2000) 260.

[13] KORALZ version 4.04 is used;
S. Jadach, B. F. L. Ward and Z. Wąs, Comp. Phys. Comm. **79** (1994) 503.

[14] KORALW version 1.33 is used;
M. Skrzypek *et al.*, Comp. Phys. Comm. **94** (1996) 216.

[15] DIAG36 Monte Carlo;
F. A. Berends, P. H. Daverfeldt and R. Kleiss, Nucl. Phys. **B 253** (1985) 441.

[16] GEANT version 3.15 is used;
R. Brun *et al.*, CERN report CERN DD/EE/84-1 (1984), revised 1987.

[17] H. Fesefeldt, RWTH Aachen report PITHA 85/2 (1985).

[18] P. Béné *et al.*, Nucl. Inst. Meth. **A 306** (1991) 150;
D. Haas *et al.*, Nucl. Inst. Meth. **A 420** (1991) 101.

[19] R. Bizzarri *et al.*, Nucl. Instr. Meth. **A 283** (1989) 799.

[20] L3 Collab., M. Acciarri *et al.*, Phys. Lett. **B 519** (2001) 33.

The L3 Collaboration:

P.Achard,[20] O.Adriani,[17] M.Aguilar-Benitez,[24] J.Alcaraz,[24] G.Alemanni,[22] J.Allaby,[18] A.Aloisio,[28] M.G.Alviggi,[28]
H.Anderhub,[46] V.P.Andreev,[6,33] F.Anselmo,[8] A.Arefiev,[27] T.Azemoon,[3] T.Aziz,[9] P.Bagnaia,[38] A.Bajo,[24] G.Baksay,[25]
L.Baksay,[25] S.V.Baldew,[2] S.Banerjee,[9] Sw.Banerjee,[4] A.Barczyk,[46,44] R.Barillère,[18] P.Bartalini,[22] M.Basile,[8]
N.Batalova,[43] R.Battiston,[32] A.Bay,[22] F.Becattini,[17] U.Becker,[13] F.Behner,[46] L.Bellucci,[17] R.Berbeco,[3] J.Berdugo,[24]
P.Berges,[13] B.Bertucci,[32] B.L.Betev,[46] M.Biasini,[32] M.Biglietti,[28] A.Biland,[46] J.J.Blaising,[4] S.C.Blyth,[34] G.J.Bobbink,[2]
A.Böhm,[1] L.Boldizsar,[12] B.Borgia,[38] S.Bottai,[17] D.Bourilkov,[46] M.Bourquin,[20] S.Braccini,[20] J.G.Branson,[40]
F.Brochu,[4] J.D.Burger,[13] W.J.Burger,[32] X.D.Cai,[13] M.Capell,[13] G.Cara Romeo,[8] G.Carlino,[28] A.Cartacci,[17]
J.Casaus,[24] F.Cavallari,[38] N.Cavallo,[35] C.Cecchi,[32] M.Cerrada,[24] M.Chamizo,[20] Y.H.Chang,[48] M.Chemarin,[23]
A.Chen,[48] G.Chen,[7] G.M.Chen,[7] H.F.Chen,[21] H.S.Chen,[7] G.Chiefari,[28] L.Cifarelli,[39] F.Cindolo,[8] I.Clare,[13] R.Clare,[37]
G.Coignet,[4] N.Colino,[24] S.Costantini,[38] B.de la Cruz,[24] S.Cucciarelli,[32] J.A.van Dalen,[30] R.de Asmundis,[28]
P.Déglon,[20] J.Debreczeni,[12] A.Degré,[4] K.Dehmelt,[25] K.Deiters,[44] D.della Volpe,[28] E.Delmeire,[20] P.Denes,[36]
F.DeNotaristefani,[38] A.De Salvo,[46] M.Diemoz,[38] M.Dierckxsens,[2] C.Dionisi,[38] M.Dittmar,[46] A.Doria,[28] M.T.Dova,[10,♯]
D.Duchesneau,[4] M.Duda,[1] B.Echenard,[20] A.Eline,[18] A.El Hage,[1] H.El Mamouni,[23] A.Engler,[34] F.J.Eppling,[13]
P.Extermann,[20] M.A.Falagan,[24] S.Falciano,[38] A.Favara,[31] J.Fay,[23] O.Fedin,[33] M.Felcini,[46] T.Ferguson,[34] H.Fesefeldt,[1]
E.Fiandrini,[32] J.H.Field,[20] F.Filthaut,[30] P.H.Fisher,[13] W.Fisher,[36] I.Fisk,[40] G.Forconi,[13] K.Freudenreich,[46]
C.Furetta,[26] Yu.Galaktionov,[27,13] S.N.Ganguli,[9] P.Garcia-Abia,[24] M.Gataullin,[31] S.Gentile,[38] S.Giagu,[38] Z.F.Gong,[21]
G.Grenier,[23] O.Grimm,[46] M.W.Gruenewald,[16] M.Guida,[39] R.van Gulik,[2] V.K.Gupta,[36] A.Gurtu,[9] L.J.Gutay,[43]
D.Haas,[5] D.Hatzifotiadou,[8] T.Hebbeker,[1] A.Hervé,[18] J.Hirschfelder,[34] H.Hofer,[46] M.Hohlmann,[25] G.Holzner,[46]
S.R.Hou,[48] Y.Hu,[30] B.N.Jin,[7] L.W.Jones,[3] P.de Jong,[2] I.Josa-Mutuberría,[24] M.Kaur,[14] M.N.Kienzle-Focacci,[20]
J.K.Kim,[42] J.Kirkby,[18] W.Kittel,[30] A.Klimentov,[13,27] A.C.König,[30] M.Kopal,[43] V.Koutsenko,[13,27] M.Kräber,[46]
R.W.Kraemer,[34] A.Krüger,[45] A.Kunin,[13] P.Ladron de Guevara,[24] I.Laktineh,[23] G.Landi,[17] M.Lebeau,[18] A.Lebedev,[13]
P.Lebrun,[23] P.Lecomte,[46] P.Lecoq,[18] P.Le Coultre,[46] J.M.Le Goff,[18] R.Leiste,[45] M.Levtchenko,[26] P.Levtchenko,[33]
C.Li,[21] S.Likhoded,[45] C.H.Lin,[48] W.T.Lin,[48] F.L.Linde,[2] L.Lista,[28] Z.A.Liu,[7] W.Lohmann,[45] E.Longo,[38] Y.S.Lu,[7]
C.Luci,[38] L.Luminari,[38] W.Lustermann,[46] W.G.Ma,[21] L.Malgeri,[20] A.Malinin,[27] C.Maña,[24] J.Mans,[36] J.P.Martin,[23]
F.Marzano,[38] K.Mazumdar,[9] R.R.McNeil,[6] S.Mele,[18,28] L.Merola,[28] M.Meschini,[17] W.J.Metzger,[30] A.Mihul,[11]
H.Milcent,[18] G.Mirabelli,[38] J.Mnich,[1] G.B.Mohanty,[9] G.S.Muanza,[23] A.J.M.Muijs,[2] B.Musicar,[40] M.Musy,[38] S.Nagy,[15]
S.Natale,[20] M.Napolitano,[28] F.Nessi-Tedaldi,[46] H.Newman,[31] A.Nisati,[38] T.Novak,[30] H.Nowak,[45] R.Ofierzynski,[46]
G.Organtini,[38] I.Pal,[43] C.Palomares,[24] P.Paolucci,[28] R.Paramatti,[38] G.Passaleva,[17] S.Patricelli,[28] T.Paul,[10]
M.Pauluzzi,[32] C.Paus,[13] F.Pauss,[46] M.Pedace,[38] S.Pensotti,[26] D.Perret-Gallix,[4] B.Petersen,[30] D.Piccolo,[28] F.Pierella,[8]
M.Pioppi,[32] P.A.Piroué,[36] E.Pistolesi,[26] V.Plyaskin,[27] M.Pohl,[20] V.Pojidaev,[17] J.Pothier,[18] D.Prokofiev,[33]
J.Quartieri,[39] G.Rahal-Callot,[46] M.A.Rahaman,[9] P.Raics,[15] N.Raja,[9] R.Ramelli,[46] P.G.Rancoita,[26] R.Ranieri,[17]
A.Raspereza,[45] P.Razis,[29] D.Ren,[46] M.Rescigno,[38] S.Reucroft,[10] S.Riemann,[45] K.Riles,[3] B.P.Roe,[3] L.Romero,[24]
A.Rosca,[45] C.Rosemann,[1] C.Rosenbleck,[1] S.Rosier-Lees,[4] S.Roth,[1] J.A.Rubio,[18] G.Ruggiero,[17] H.Rykaczewski,[46]
A.Sakharov,[46] S.Saremi,[6] S.Sarkar,[38] J.Salicio,[18] E.Sanchez,[24] C.Schäfer,[18] V.Schegelsky,[33] H.Schopper,[47]
D.J.Schotanus,[30] C.Sciacca,[28] L.Servoli,[32] S.Shevchenko,[31] N.Shivarov,[41] V.Shoutko,[13] E.Shumilov,[27] A.Shvorob,[31]
D.Son,[42] C.Souga,[23] P.Spillantini,[17] M.Steuer,[13] D.P.Stickland,[36] B.Stoyanov,[41] A.Straessner,[20] K.Sudhakar,[9]
G.Sultanov,[41] L.Z.Sun,[21] S.Sushkov,[1] H.Suter,[46] J.D.Swain,[10] Z.Szillasi,[25,¶] X.W.Tang,[7] P.Tarjan,[15] L.Tauscher,[5]
L.Taylor,[10] B.Tellili,[23] D.Teyssier,[23] C.Timmermans,[30] Samuel C.C.Ting,[13] S.M.Ting,[13] S.C.Tonwar,[9] J.Tóth,[12]
C.Tully,[36] K.L.Tung,[7] J.Ulbricht,[46] E.Valente,[38] R.T.Van de Walle,[30] R.Vasquez,[43] V.Veszpremi,[25] G.Vesztergombi,[12]
I.Vetlitsky,[27] D.Vicinanza,[39] G.Viertel,[46] S.Villa,[37] M.Vivargent,[4] S.Vlachos,[5] I.Vodopianov,[25] H.Vogel,[34] H.Vogt,[45]
I.Vorobiev,[34,27] A.A.Vorobyov,[33] M.Wadhwa,[5] Q.Wang,[30] X.L.Wang,[21] Z.M.Wang,[21] M.Weber,[18] H.Wilkens,[30]
S.Wynhoff,[36] L.Xia,[31] Z.Z.Xu,[21] J.Yamamoto,[3] B.Z.Yang,[21] C.G.Yang,[7] H.J.Yang,[3] M.Yang,[7] S.C.Yeh,[49] An.Zalite,[33]
Yu.Zalite,[33] Z.P.Zhang,[21] J.Zhao,[21] G.Y.Zhu,[7] R.Y.Zhu,[31] H.L.Zhuang,[7] A.Zichichi,[8,18,19] B.Zimmermann,[46] M.Zöller.[1]

1 III. Physikalisches Institut, RWTH, D-52056 Aachen, Germany[§]
2 National Institute for High Energy Physics, NIKHEF, and University of Amsterdam, NL-1009 DB Amsterdam, The Netherlands
3 University of Michigan, Ann Arbor, MI 48109, USA
4 Laboratoire d'Annecy-le-Vieux de Physique des Particules, LAPP,IN2P3-CNRS, BP 110, F-74941 Annecy-le-Vieux CEDEX, France
5 Institute of Physics, University of Basel, CH-4056 Basel, Switzerland
6 Louisiana State University, Baton Rouge, LA 70803, USA
7 Institute of High Energy Physics, IHEP, 100039 Beijing, China[△]
8 University of Bologna and INFN-Sezione di Bologna, I-40126 Bologna, Italy
9 Tata Institute of Fundamental Research, Mumbai (Bombay) 400 005, India
10 Northeastern University, Boston, MA 02115, USA
11 Institute of Atomic Physics and University of Bucharest, R-76900 Bucharest, Romania
12 Central Research Institute for Physics of the Hungarian Academy of Sciences, H-1525 Budapest 114, Hungary[‡]
13 Massachusetts Institute of Technology, Cambridge, MA 02139, USA
14 Panjab University, Chandigarh 160 014, India
15 KLTE-ATOMKI, H-4010 Debrecen, Hungary[¶]
16 Department of Experimental Physics, University College Dublin, Belfield, Dublin 4, Ireland
17 INFN Sezione di Firenze and University of Florence, I-50125 Florence, Italy
18 European Laboratory for Particle Physics, CERN, CH-1211 Geneva 23, Switzerland
19 World Laboratory, FBLJA Project, CH-1211 Geneva 23, Switzerland
20 University of Geneva, CH-1211 Geneva 4, Switzerland
21 Chinese University of Science and Technology, USTC, Hefei, Anhui 230 029, China[△]
22 University of Lausanne, CH-1015 Lausanne, Switzerland
23 Institut de Physique Nucléaire de Lyon, IN2P3-CNRS,Université Claude Bernard, F-69622 Villeurbanne, France
24 Centro de Investigaciones Energéticas, Medioambientales y Tecnológicas, CIEMAT, E-28040 Madrid, Spain[♭]
25 Florida Institute of Technology, Melbourne, FL 32901, USA
26 INFN-Sezione di Milano, I-20133 Milan, Italy
27 Institute of Theoretical and Experimental Physics, ITEP, Moscow, Russia
28 INFN-Sezione di Napoli and University of Naples, I-80125 Naples, Italy
29 Department of Physics, University of Cyprus, Nicosia, Cyprus
30 University of Nijmegen and NIKHEF, NL-6525 ED Nijmegen, The Netherlands
31 California Institute of Technology, Pasadena, CA 91125, USA
32 INFN-Sezione di Perugia and Università Degli Studi di Perugia, I-06100 Perugia, Italy
33 Nuclear Physics Institute, St. Petersburg, Russia
34 Carnegie Mellon University, Pittsburgh, PA 15213, USA
35 INFN-Sezione di Napoli and University of Potenza, I-85100 Potenza, Italy
36 Princeton University, Princeton, NJ 08544, USA
37 University of Californa, Riverside, CA 92521, USA
38 INFN-Sezione di Roma and University of Rome, "La Sapienza", I-00185 Rome, Italy
39 University and INFN, Salerno, I-84100 Salerno, Italy
40 University of California, San Diego, CA 92093, USA
41 Bulgarian Academy of Sciences, Central Lab. of Mechatronics and Instrumentation, BU-1113 Sofia, Bulgaria
42 The Center for High Energy Physics, Kyungpook National University, 702-701 Taegu, Republic of Korea
43 Purdue University, West Lafayette, IN 47907, USA
44 Paul Scherrer Institut, PSI, CH-5232 Villigen, Switzerland
45 DESY, D-15738 Zeuthen, Germany
46 Eidgenössische Technische Hochschule, ETH Zürich, CH-8093 Zürich, Switzerland
47 University of Hamburg, D-22761 Hamburg, Germany
48 National Central University, Chung-Li, Taiwan, China
49 Department of Physics, National Tsing Hua University, Taiwan, China

p_t (GeV)	$\langle p_t \rangle$ (GeV)	Number of Λ	Mass of Λ (MeV)	Efficiency (%)	$d\sigma/dp_t$ (pb/GeV)
0.4−0.6	0.50	3412 ± 71	1116.0 ± 0.1	10.2 ± 0.1	$273 \pm 6 \pm 36$
0.6−0.8	0.69	4408 ± 85	1115.9 ± 0.1	13.7 ± 0.1	$264 \pm 5 \pm 29$
0.8−1.0	0.89	3420 ± 81	1116.1 ± 0.1	15.3 ± 0.2	$183 \pm 4 \pm 15$
1.0−1.3	1.12	3201 ± 87	1115.7 ± 0.1	16.8 ± 0.2	$104 \pm 3 \pm 7$
1.3−1.6	1.43	1222 ± 55	1115.5 ± 0.1	17.7 ± 0.4	$38 \pm 2 \pm 3$
1.6−2.0	1.77	578 ± 41	1115.0 ± 0.2	15.9 ± 0.6	$15 \pm 1 \pm 1$
2.0−2.5	2.21	292 ± 25	1115.9 ± 0.3	17.2 ± 1.3	$6 \pm 1 \pm 1$

Table 1: The number of Λ baryons estimated by the fit, together with the Λ mass, the overall efficiency and the corresponding differential cross section as a function of p_t for $|\eta| < 1.2$. The first uncertainty on the cross section is statistical and the second systematic.

$|\eta|$	Number of Λ	Efficiency (%)	$d\sigma/d|\eta|$ (pb)
0.0−0.3	2953 ± 72	13.8 ± 0.2	$59 \pm 1 \pm 3$
0.3−0.6	2742 ± 63	13.4 ± 0.2	$56 \pm 1 \pm 3$
0.6−0.9	2904 ± 70	13.0 ± 0.2	$61 \pm 1 \pm 4$
0.9−1.2	2774 ± 89	11.1 ± 0.1	$68 \pm 2 \pm 8$

Table 2: The number of Λ baryons estimated by the fit, together with the overall efficiency and the corresponding differential cross section as a function of pseudorapidity for 0.4 GeV $< p_t \le$ 1 GeV. The first uncertainty on the cross section is statistical and the second systematic.

$|\eta|$	Number of Λ	Efficiency (%)	$d\sigma/d|\eta|$ (pb)
0.0−0.3	1458 ± 60	18.8 ± 0.5	$21 \pm 1 \pm 1$
0.3−0.6	1411 ± 62	18.2 ± 0.4	$21 \pm 1 \pm 1$
0.6−0.9	1480 ± 62	19.3 ± 0.5	$21 \pm 1 \pm 1$
0.9−1.2	1007 ± 63	14.3 ± 0.4	$19 \pm 1 \pm 3$

Table 3: The number of Λ baryons estimated by the fit, together with the overall efficiency and the corresponding differential cross section as a function of pseudorapidity for 1 GeV $< p_t <$ 2.5 GeV. The first uncertainty on the cross section is statistical and the second systematic.

10

p_t (GeV)	Background subtraction (%)	Scales and resolutions (%)	Monte Carlo modelling (%)	Trigger efficiency (%)	Total (%)
0.4−0.6	12.1	4.2	1.4	2.0	13.0
0.6−0.8	9.8	4.2	1.6	2.0	11.0
0.8−1.0	6.6	4.2	1.9	2.0	8.3
1.0−1.3	5.3	4.2	2.1	2.0	7.3
1.3−1.6	5.8	4.2	2.4	2.0	7.8
1.6−2.0	6.4	4.2	2.8	2.0	8.4
2.0−2.5	19.4	4.2	4.8	2.0	20.5

Table 4: Systematic uncertainty on the cross section of the $e^+e^- \rightarrow e^+e^-\Lambda X$ and $e^+e^- \rightarrow e^+e^-\overline{\Lambda}X$ processes due to background subtraction, scales and resolution uncertainties, Monte Carlo modelling and trigger efficiency. The total systematic uncertainty is the quadratic sum of the different contributions.
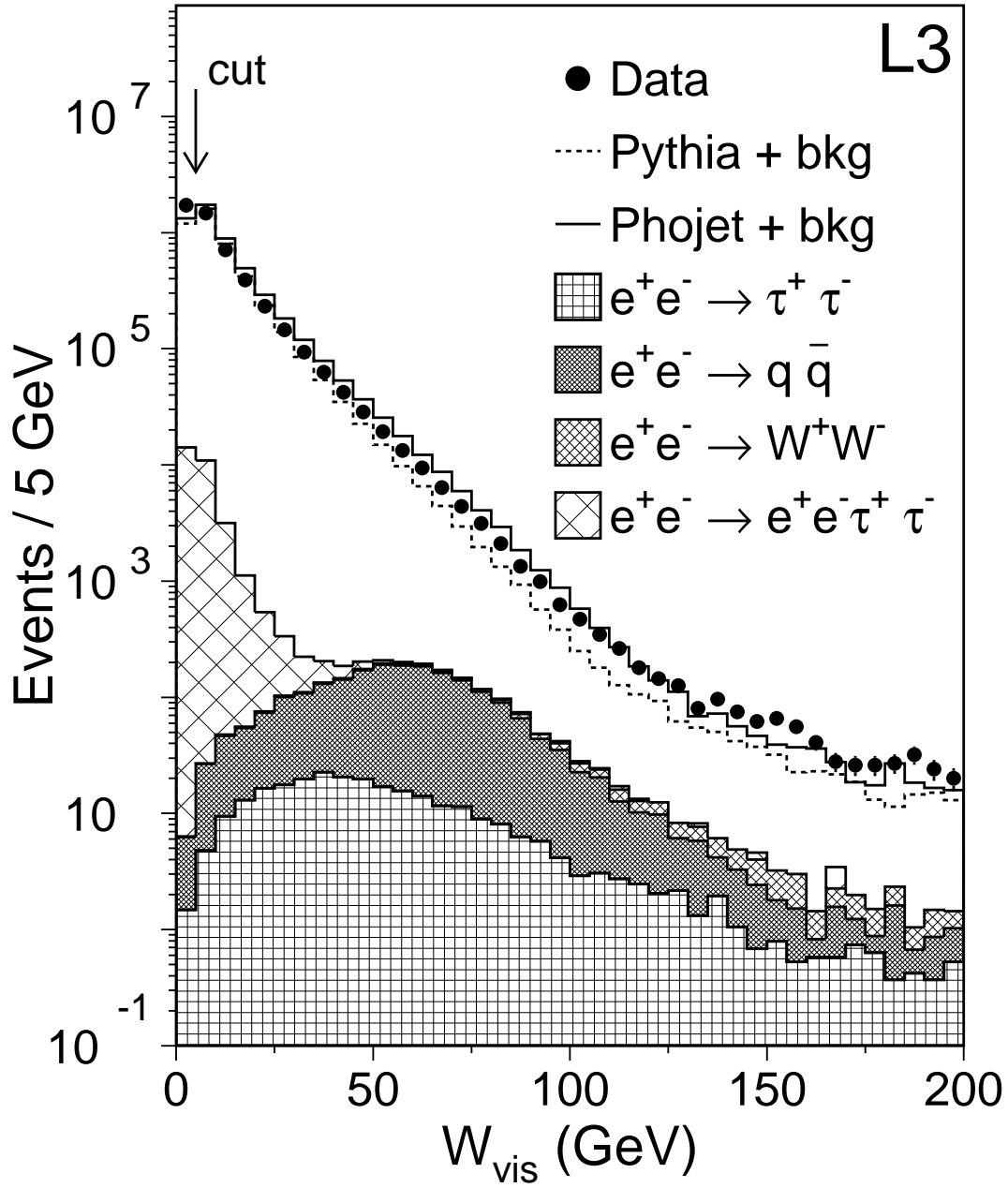
Figure 1: The distribution of the visible mass W_{vis}. The Monte Carlo distributions are normalized to the data luminosity. Various contributions to the background (bkg) are shown as cumulative histograms.
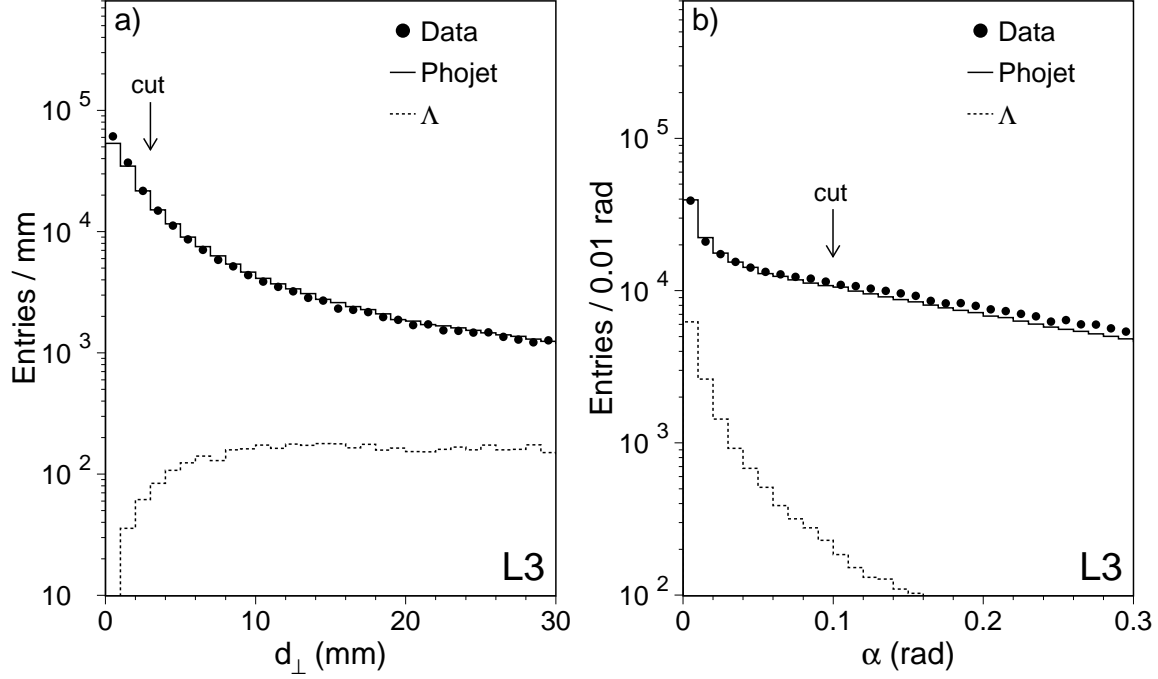
Figure 2: Distribution of the variables used for the selection of secondary vertices: a) the distance, in the plane transverse to the beam direction, between the secondary vertex and the primary e^+e^- interaction point, $d_\perp$, and b) the angle between the total transverse momentum vector of the two outgoing tracks and the direction in the transverse plane between the primary interaction point and the secondary vertex, α. In each plot, all other selection criteria are applied. The predictions of the PHOJET Monte Carlo are shown as the full line and the contribution due to Λ baryons as the dashed line. The Monte Carlo distributions are normalized to the data luminosity.

13
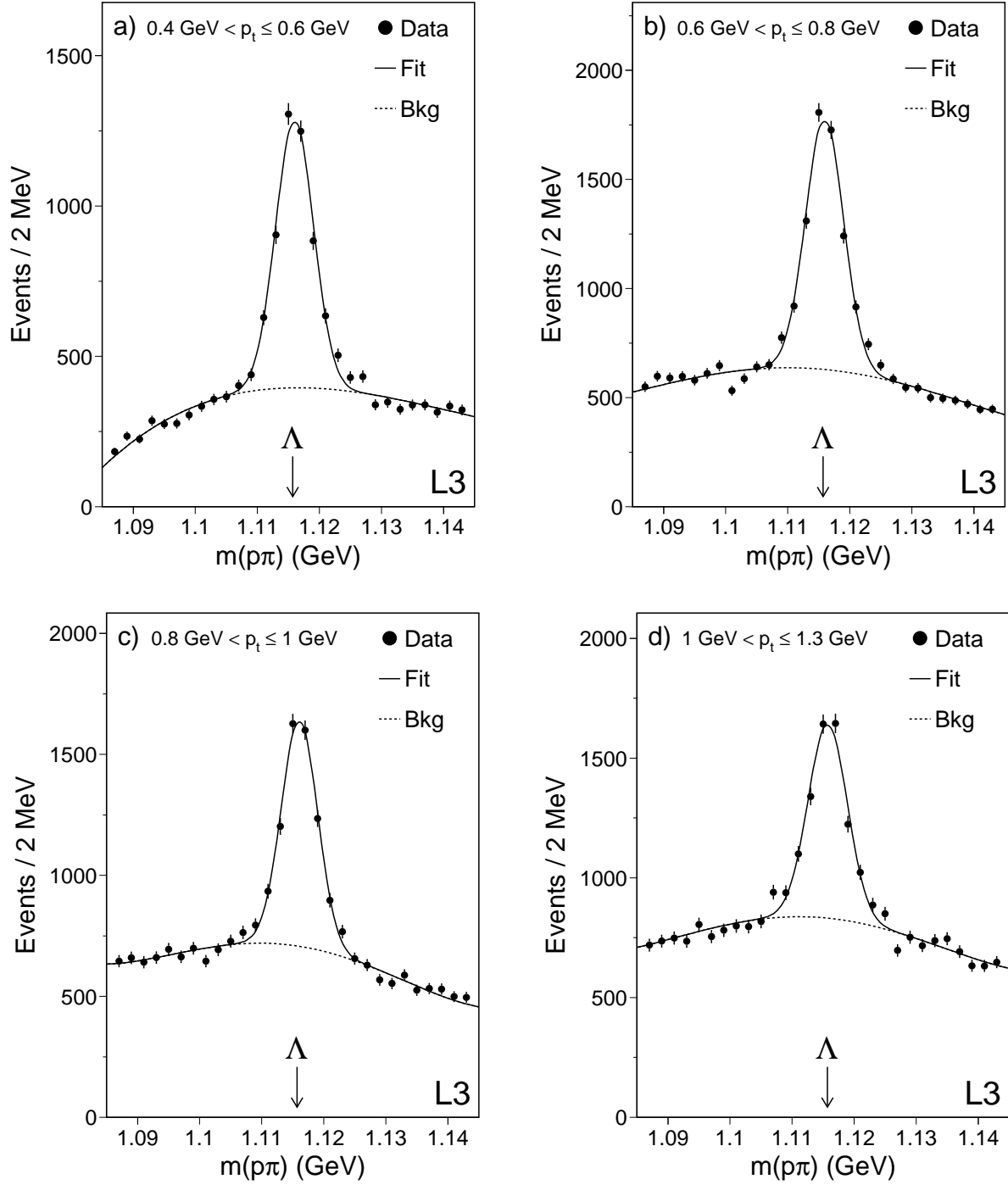
Figure 3: The invariant mass of the pπ system for a) 0.4 GeV $< p_t \leq$ 0.6 GeV, b) 0.6 GeV $<$ $p_t \leq$ 0.8 GeV, c) 0.8 GeV $< p_t \leq$ 1 GeV and d) 1 GeV $< p_t \leq$ 1.3 GeV . The signal is modelled with a Gaussian and the background by a fourth-degree Chebyshev polynomial.

14

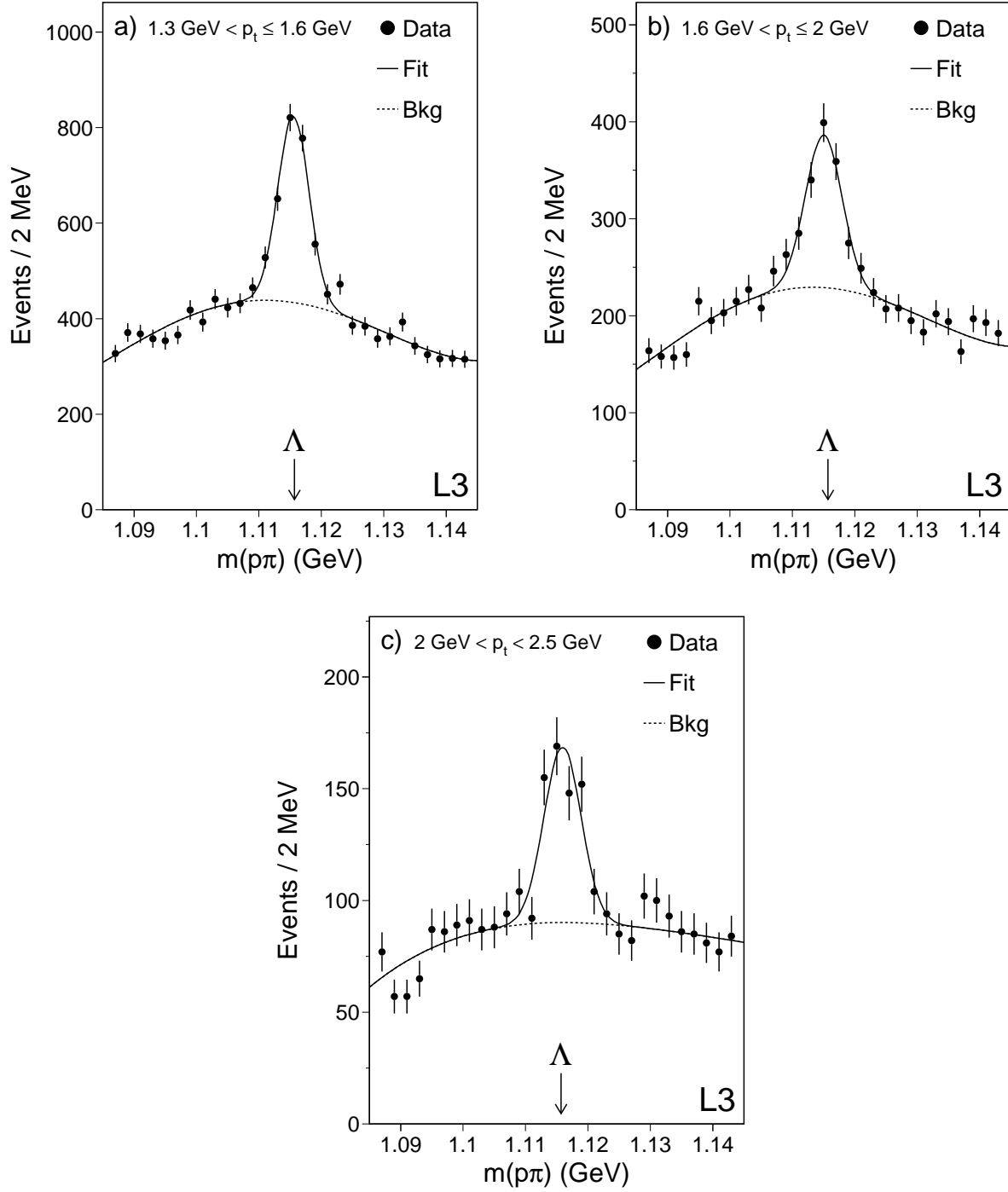Figure 4: The invariant mass of the pπ system for a) 1.3 GeV $< p_t \leq$ 1.6 GeV, b) 1.6 GeV $<$ $p_t \leq$ 2 GeV and c) 2 GeV $< p_t <$ 2.5 GeV. The signal is modelled with a Gaussian and the background by a fourth order Chebyshev polynomial.
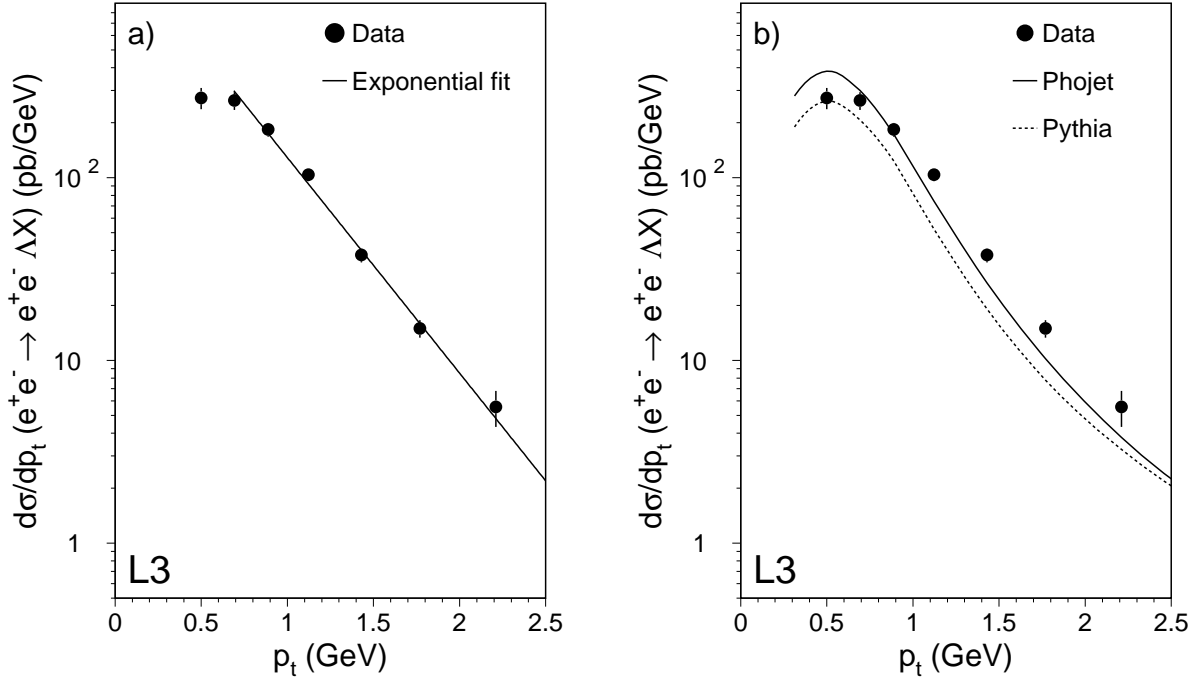
Figure 5: The differential cross section as a function of p_t for the $e^+e^- \to e^+e^-\Lambda X$ and $e^+e^- \to e^+e^-\overline{\Lambda}X$ processes for $|\eta| < 1.2$: a) with the exponential fit described in the text and b) compared to the predictions of the PHOJET and PYTHIA Monte Carlo programs.
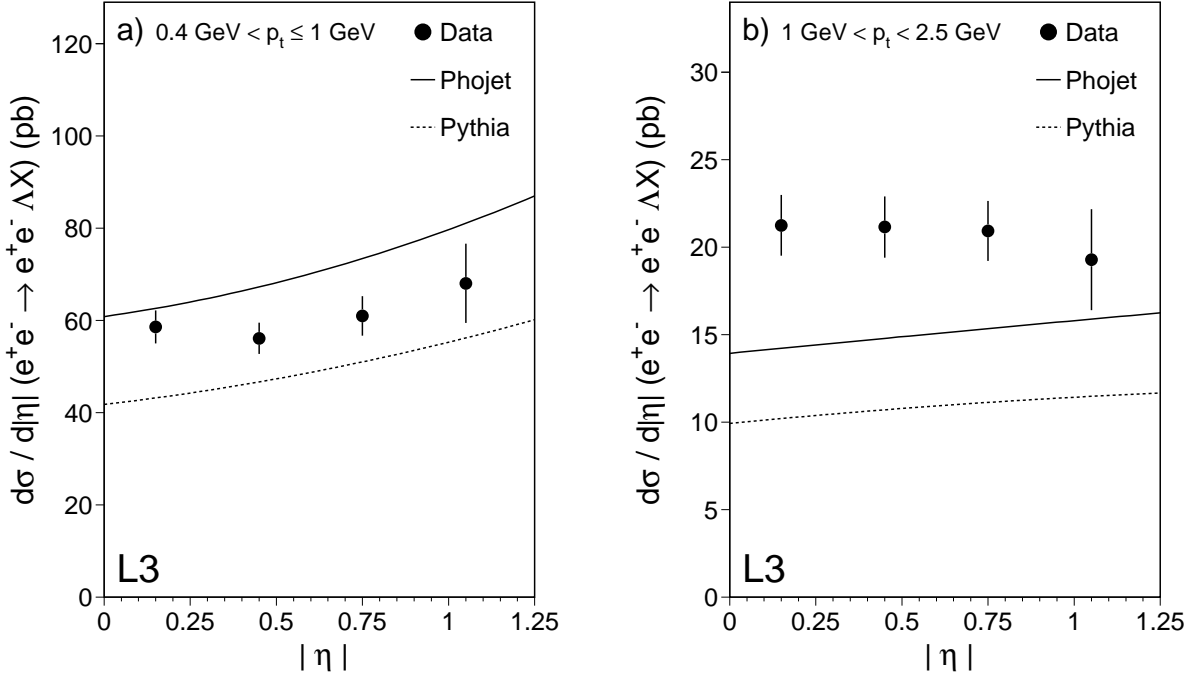

Figure 6: The differential cross section as a function of $|\eta|$ for the $e^+e^- \to e^+e^-\Lambda X$ and $e^+e^- \to e^+e^-\overline{\Lambda}X$ processes for: a) $0.4 \text{ GeV} < p_t \leq 1 \text{ GeV}$ and b) $1 \text{ GeV} < p_t < 2.5 \text{ GeV}$. The data are compared to the predictions of the PHOJET and PYTHIA Monte Carlo programs.

16